



# Spectral Nudging Impacts on Precipitation Downscaling in the Conformal Cubic Atmospheric Model, version CCAM-2504: Insights from Summer 2011

Son C. H. Truong<sup>1</sup>, Marcus J. Thatcher<sup>1</sup>, Phuong Loan Nguyen<sup>2</sup>, Lisa V. Alexander<sup>2,3</sup>  
5 and John L. McGregor<sup>1</sup>

<sup>1</sup> The Commonwealth Scientific and Industrial Research Organisation, Victoria, Australia

<sup>2</sup> Climate Change Research Centre, UNSW Sydney, NSW, Australia

<sup>3</sup> ARC Centre of Excellence for the Weather of the 21<sup>st</sup> Century, UNSW Sydney, NSW, Australia

*Correspondence to:* Son C. H. Truong (sonny.truong@csiro.au)

10 **Abstract.** This study evaluates the impacts of spectral nudging on rainfall when dynamically downscaling with the Conformal Cubic Atmospheric Model (CCAM). The study focuses on the extreme 2010 – 11 La Niña, in conjunction with the Madden – Julian Oscillation (MJO), across the CORDEX – Australasia domain at 12.5 km with CCAM nested in ERA-5 reanalysis. Sixteen simulations were performed, systematically varying nudging wavelength, vertical extent, frequency, and variable choice, and evaluated against GPM-IMERG precipitation and ERA5 reanalysis. Configurations at short nudging 15 wavelengths (~500 – 1500 km), with high-frequency updates (1h), and including pressure, wind and temperature delivered the most robust performance. These setups reduced large-scale rainfall biases, improved spatial and temporal correlations, reproduced vertical structure and moisture convergence more realistically, and achieved the closest agreement with observed mean and extreme observed rainfall. In contrast, coarse-scale (3000 km), full-column constraints, or nudging limited to pressure or wind variables degraded performance, producing oversmoothed variability, misplaced convection, and unrealistic 20 rainfall patterns. Overall, the results demonstrate that carefully tuned spectral nudging enhances the fidelity of both mean and extreme rainfall in CCAM, while preserving large-scale teleconnections associated with La Niña, MJO, and retaining mesoscale variability. This study strengthens confidence in CCAM downscaling for CORDEX – Australasia, with implications extending to other CORDEX domains and applications.

## 1 Introduction

25 The accurate assessment of regional climate variability and extremes is essential for supporting climate change adaptation and risk management efforts (IPCC, 2021). While general circulation models (GCMs) provide valuable insights into large-scale climate dynamics, their coarse resolution and simplified representation of regional processes limit their ability to capture local climate features, particularly extremes such as heavy rainfall events (Giorgi and Mearns, 1999; Nguyen et al., 2024). To overcome this limitation, regional climate models (RCMs) offer higher spatial resolution and a more detailed 30 representation of topography and regional processes (Giorgi, 2019). Numerous studies have evaluated RCM performance



over Australasia, demonstrating skill in reproducing regional climate features (Chapman et al., 2024; Schroeter et al., 2024; Sugata et al., 2025).

A central challenge for RCMs efficiently assimilates the relevant large-scale atmospheric circulation from the coarse-resolution model (e.g., forcing from host GCMs) to the RCMs (von Storch et al., 2000; Feser et al., 2012). Without 35 constraints, model biases can grow within the regional domain, resulting in considerable discrepancies from the large-scale circulations (Miguez-Macho et al., 2004). To address this, a scale-selective technique (e.g., spectral nudging) was introduced to constrain the state of the regional atmosphere at large length scales in spectral space (Von Storch et al., 2000; Kanamaru and Kanamitsu 2007; Thatcher and McGregor, 2008). This approach allows RCMs to develop small-scale features superimposed on the large-scale atmospheric conditions from GCMs. Studies have shown that spectral nudging improves 40 mean and extreme precipitation (Wang and Kotamarthi, 2013; Omrani et al., 2015), tropical cyclone statistics (Choi and Lee, 2015; Jin et al., 2016) and low-level wind circulation (Tang et al., 2017). Spectral nudging has also been shown to outperform other techniques, such as grid nudging, particularly in simulating extreme rainfall and low-level circulation (Liu et al., 2012; Yang et al., 2019).

The effectiveness of spectral nudging depends critically on configuration choices such as wavelengths, update frequency, 45 vertical level, and the variables being constrained (Alexandru et al., 2009; Omrani et al., 2015). These parameters regulate the interplay between large-scale constraint from GCMs and internal RCMs adjustment that can pose a substantial impact of the simulated circulation and precipitation. Gómez and Miguez-Macho (2017) demonstrated that nudging with wavelengths around 1000 km yields optimal results as shorter wavelengths tend to suppress fine-scale variability whereas larger wavelengths may distort synoptic conditions (Spero et al., 2018). The update frequency influences the tracks and 50 intensification of tropical cyclone (Feser and Barcikowska., 2012; Cha et al., 2011). Moisture nudging is a debated technique. Some research cautions against it due to thermodynamic inconsistencies where temperature, moisture, and dynamical fields are no longer physically aligned when the RCM is nudged toward the host GCM (Heikkila et al., 2010; Otte et al., 2012; Menut et al., 2024), while other studies suggest it can enhance precipitation simulation (Spero et al., 2014). The selection of vertical level at which RCMs are being nudged, or nudging profile, is primarily empirical, as different 55 formulations can lead to various outcomes (von Storch et al., 2000; Miguez-Macho et al., 2005; Hong and Chang, 2012; Tang et al., 2017). While RCM performance has been evaluated in Australasia (Liu et al., 2024; Ma et al., 2025; Truong and Thatcher, 2025), to the best of our knowledge, no studies have systematically examined the sensitivity of spectral nudging configurations, in contrast to more extensive investigations over East Asia (Tang et al., 2009; Yhang and Hong, 2011), Europe (Feser, 2012), and North America (Castro et al., 2005).

60 This study evaluates the impacts of different spectral nudging configurations on rainfall when dynamically downscaling with the Conformal Cubic Atmospheric Model (CCAM) during the extreme 2010 – 11 La Niña, in conjunction with the Madden– Julian Oscillation (MJO) and the Australian monsoon (Cai and van Renssch, 2012; Evans and Boyer-Souchet, 2012; Lisonbee and Ribbe 2021), across the CORDEX – Australasia domain. This 2010 – 11 La Niña season serves as a stringent test of CCAM’s performance, as it was among the strongest La Niña events in Australia’s meteorological record, rivalling



65 historical extremes (BoM, 2012) led to widespread flooding in many regions over Australia including Queensland, Victoria, New South Wales, and Western Australia (Ummenhofer et al. 2015). The season was also marked by increased tropical cyclone activity, notably severe tropical cyclone Carlos over Darwin (367.6 mm/day) and Yasi over Queensland (471 mm/day). In this study, we aim to:

1. Evaluate the ability of CCAM to reproduce regional rainfall and large-scale circulation during the extreme 2010 – 70 11 La Niña;
2. Quantify the influence of nudging parameter choices on the representation of mean and extreme rainfall; and
3. Identify parameter combinations that improve the fidelity of regional rainfall simulations over Australasia.

The paper is organized as follows: Section 2 outlines the data and methods; Section 3 describes study results; and Section 4 discusses the findings and conclusions.

## 75 2 Data and methods

### 2.1 ERA5 reanalysis

The ERA5 reanalysis, produced by the European Center for Medium-Range Weather Forecasts (ECMWF), is based on the global Numerical Weather Prediction (NWP) model Integrated Forecast System (IFS) version CY41R2 (Hersbach et al., 2020). The model provides hourly estimates of atmospheric variables, at a horizontal resolution of 31 km and 137 vertical 80 levels from the surface to 0.01 hPa. The data is available on both surface (e.g., total precipitation) and 37 pressure levels (e.g., vertical winds). The variables used in this study are wind speed, temperature, specific humidity, and mean sea level pressure.

### 2.2 Observations

In this study, we evaluate simulated precipitation using the Integrated Multi-satellite Retrievals for the Global Precipitation 85 Measurement IMERG Final Run product (Version 07; Huffman et al., 2019), distributed by NASA GES DISC. The level-3 IMERG fields provide  $0.1^\circ \times 0.1^\circ$  coverage from  $60^\circ\text{S}$ - $60^\circ\text{N}$  and merge estimates from a constellation of passive-microwave and infrared sensors, intercalibrated to monthly rain-gauge analyses; we use the daily accumulation ( $\text{mm day}^{-1}$ ). To benchmark observational uncertainty, particularly pronounced over the equatorial and data sparse regions (Alexander et al. 2025; Nguyen et al., 2022), we include two additional daily products: the Global Precipitation Climatology Project (GPCP) 90 daily CDR v3.2 (Huffman et al., 2023) and the Climate Prediction Center morphing method (CMORPH) v1.0 CRT (Joyce et al., 2004; Xie et al., 2017). The GPCP v3.2 provides globally complete  $0.5^\circ \times 0.5^\circ$  analyses from June 2000 to present, blending low-orbit satellite microwave data, geosynchronous-orbit satellite infrared data, sounder-based estimates, and surface rain gauge observations. The CMORPH v1.0 CRT provides bias-corrected, reprocessed estimates on a  $0.25^\circ$  grid with native 30-min resolution aggregated to daily for 1998-2023. As a high-quality continental reference over Australia, we 95 also use AGCD v1.0.0 daily rainfall, a  $0.05^\circ \times 0.05^\circ$  gridded gauge-based analysis derived from quality-controlled station



data across mainland Australia and Tasmania (Jones et al., 2009). These datasets are selected for their demonstrated consistency in representing daily precipitation (Imran and Eván 2025) and extremes (Alexander et al., 2020; Nguyen et al., 2020).

### 2.3 Model description

100 The climate model used for the study is Conformal Cubic Atmospheric Model (CCAM) (McGregor and Dix, 2008), developed by the Commonwealth Scientific and Industrial Research Organisation (CSIRO). CCAM is an open-source global stretched-grid non-hydrostatic numerical model, which has been extensively used for regional climate studies (Gibson et al., 2024, Liu et al., 2024; Sugata et al., 2025). CCAM can be operated with either a stretched grid or with a global quasi-uniform grid (Truong et al., 2025), driven by sea-surface temperatures (SSTs) and sea ice concentrations (Hoffmann et al., 105 2016). This makes CCAM useful for regional climate simulations where errors arising from lateral boundary conditions can be avoided, although physical parameterisations must operate successfully over a range of spatial scales. The amount of stretching is described by a Schmidt factor where 1 indicates a quasi-uniform grid and values greater than 1 imply an increasing amount of grid stretching. CCAM includes parameterisations for radiation (Freidenreich and Ramaswamy, 1999; Schwarzkopf and Ramaswamy, 1999), convection (McGregor, 2003), gravity wave drags (Chouinard et al., 1986), and 110 boundary layer turbulent mixing (Hurley, 2007). CCAM also includes the CABLE land-surface scheme (Kowalczyk et al., 2006), the UCLEM urban parameterisation (Thatcher and Hurley, 2011) and a cloud microphysics scheme based on Rotstayn (1997). Thatcher and McGregor (2008) introduced a scale-selective filtering approach (e.g., spectral nudging), based on convolution-based scheme, for CCAM that constrains only the large length scales while allowing regional atmosphere at small length scales to evolve freely.

### 115 2.4 Model configuration

To assess the impacts of spectral nudging on precipitation, a total of 16 simulations were conducted using CCAM arranged into seven groups (Table 1). “*Ctrl*” group includes no nudging. “*P\_var*” group comprised three simulations (P\_3000\_1h\_L0.85, P\_1500\_1h\_L0.85, and P\_0500\_1h\_L0.85) in which only surface pressure was spectrally nudged above the planetary boundary layer (PBL) at wavelengths of 500, 1500, and 3000 km, with a relaxation interval of 1h. In “*PUV*” 120 group, both surface pressure and horizontal wind components were nudged at the same wavelengths and interval. “*PUVT\_1h*” group extended nudging variables to include surface pressure, horizontal wind, and temperature, while “*PUVT\_3h*” group used identical variables and wavelengths but a weaker nudging strength, with the relaxation interval increased to 3h. “*PUVT\_L*” group tested the sensitivity to vertical level at which nudging is applied, including (i) full-column (L1, surface to top of the atmosphere), and (ii) half column (L0.5, mid to top of the atmosphere). Finally, “*PUVTQ*” 125 simulation nudged surface pressure, horizontal wind, temperature, and specific humidity with a wavelength of 3000 km. The simulations are initialised using ERA5 reanalysis at 00 UTC on November 1, 2010, and run for a period of 5 months at 12



km horizontal resolution and 54 vertical level. A 1-month spin-up period is used to stabilise the model. The SST evolution is driven from ERA5 reanalysis.

**Table 1 Summary of the 16 simulations conducted in this study. Each simulation differs based on four key nudging options: variables (pressure [p], zonal and meridional wind components [u] and [v], temperature [t], and specific humidity [q]), horizontal wavelength (in km), update frequency (in hours), and vertical level. Simulation names follow the format: [VARs]\_[Wavelength]\_[Frequency]\_[Level], where “VARs” represents the nudged variables (e.g., PUVTQ), “Wavelength” is the horizontal nudging wavelength (e.g., 3000 km), “Frequency” is the update interval (e.g., 1h), and “Level” indicates the vertical level at which the model being nudged to the top of the atmosphere (e.g., 0.85 for 0.85 sigma level). The simulations are grouped by nudging configuration to facilitate comparison.**

EXP. group	EXP.	EXP. name	Nudging variables	Wavelength (km)	Update frequency	Level
CTL	1	Ctrl	-	-	-	-
P_var	2	P_3000_1h_L0.85	p	3000	1h	0.85
	3	P_1500_1h_L0.85		1500	1h	0.85
	4	P_0500_1h_L0.85		500	1h	0.85
PUV	5	PUV_3000_1h_L0.85	p, u, v	3000	1h	0.85
	6	PUV_1500_1h_L0.85		1500	1h	0.85
	7	PUV_0500_1h_L0.85		500	1h	0.85
PUVT_1h	8	PUVT_3000_1h_L0.85	p, u, v, t	3000	1h	0.85
	9	PUVT_1500_1h_L0.85		1500	1h	0.85
	10	PUVT_0500_1h_L0.85		500	1h	0.85
PUVT_3h	11	PUVT_3000_3h_L0.85	p, u, v, t	3000	3h	0.85
	12	PUVT_1500_3h_L0.85		1500	3h	0.85
	13	PUVT_0500_3h_L0.85		500	3h	0.85
PUVT_L	14	PUVT_3000_1h_L0.5	p, u, v, t	3000	1h	0.5
	15	PUVT_3000_1h_L1	p, u, v, t	3000	1h	1
PUVTQ	16	PUVTQ_3000_1h_L0.85	p, u, v, t, q	3000	1h	0.85

Ispphording et al. (2024) introduce a set of minimum standard metrics benchmarking regional climate model in estimating four fundamental characteristics (intensity, spatial distribution, seasonal cycle and changes over time) of rainfall over Australia. Here, we adopted the mean absolute percentage error (MAPE) and the spatial correlation coefficient (Scor) as other two metrics not being relevant given the short simulation that we are performing. The MAPE is defined following Eq.

140 (1)

$$\text{MAPE} = \frac{1}{n} \sum_{i=1}^n \frac{|\text{model}_i - \text{obs}_i|}{\text{obs}_i} \quad (1)$$

, where n is the number of grid cells in the spatial domain. Scor quantifies pattern alignment, ranging from 0 (no match) to 1 (perfect match). In addition to precipitation-based metrics, we also examined the large-scale moisture transport by calculating the divergence of water vapor flux at 700 hPa. The water vapor flux divergence is defined following Eq. (2)



145  $\nabla(Vq) = \frac{\partial}{\partial x}(uq) + \frac{\partial}{\partial y}(vq)$  (2)

where  $q$  denotes the specific humidity, and  $u$  and  $v$  are the zonal and meridional wind components, respectively.

### 3 Results

#### 3.1 Mean precipitation

##### 3.1.1 Spatial variability of precipitation

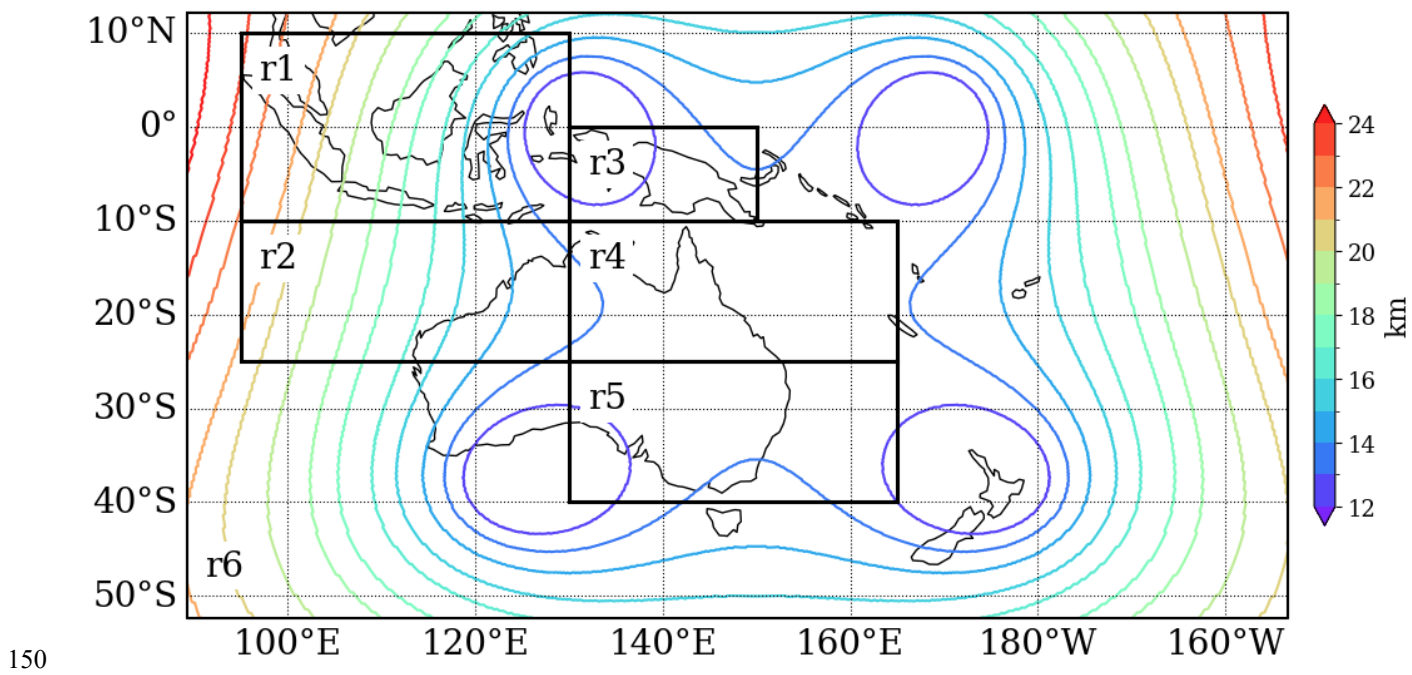
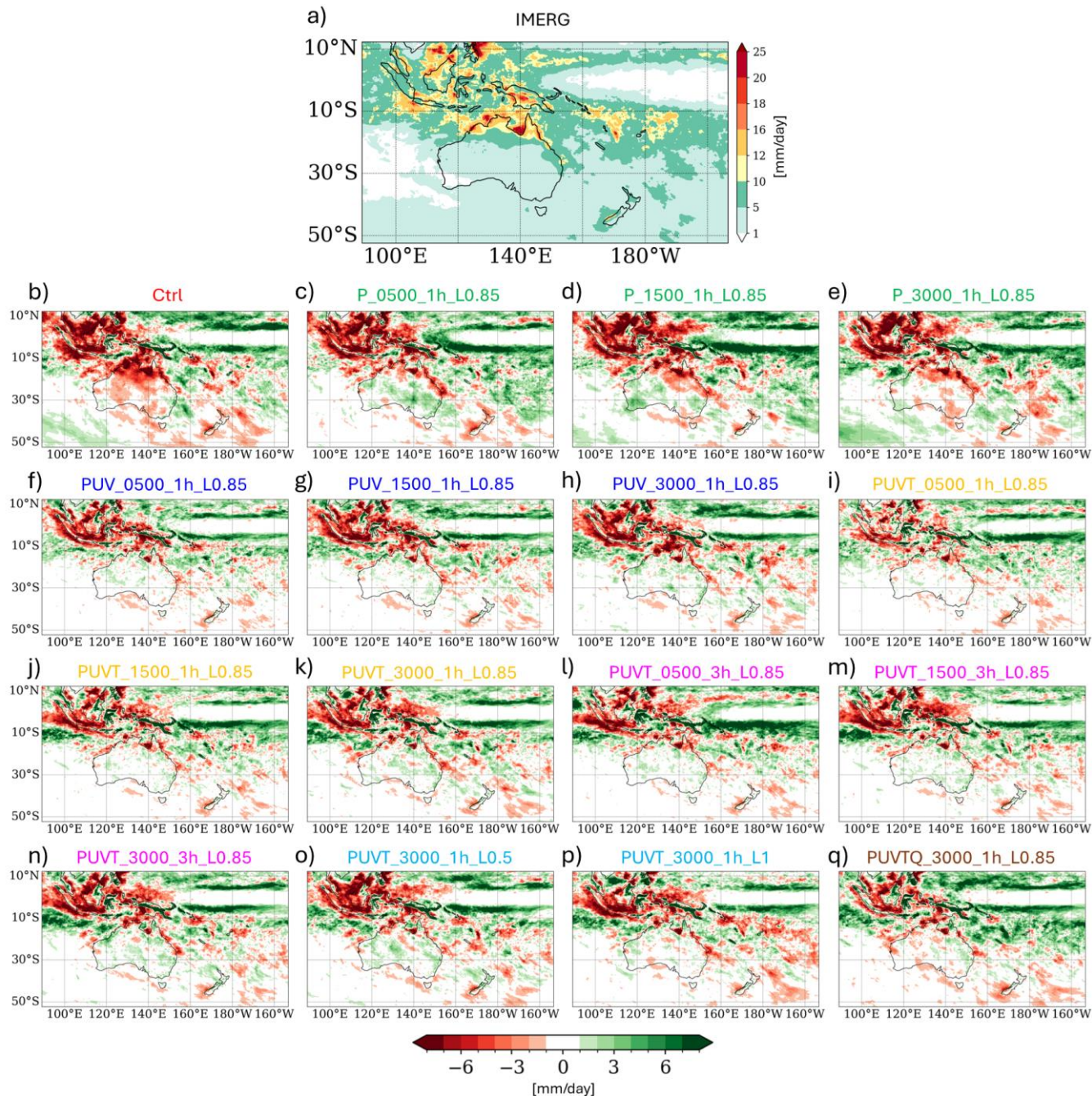


Figure 1 CCAM simulation domain with grid resolution ranging from 12 to 25 km, shown in contour colours. The study domain is divided into six subregions, labelled R1 to R6, representing the Maritime Continent, northwest Australia, southwestern pacific, northeast Australia, southeast Australia, and the whole simulated domain ( $50^{\circ}\text{S}$  –  $10^{\circ}\text{N}$ ,  $90^{\circ}\text{E}$  –  $150^{\circ}\text{W}$ ), respectively.

155 To facilitate our regional analysis, the CORDEX–Australasia domain is partitioned into three subregions (R2, R4, and R5), which represent distinct climatic and synoptic regimes: R2 (northwestern Australia), R4 (northeastern Australia), and R5 (southeastern Australia) (Fig. 1). We also include the Maritime Continent (MC) and the southwestern pacific as R1 and R3 to examine the mean and extreme precipitation over these regions albeit the R1 and R3 belong to the CORDEX – SEA domain. Finally, R6 is defined as the entire domain. This subregional framework provides a consistent basis for examining



160 precipitation processes across a broad spectrum of climatic drivers, including tropical–extratropical interactions, the Madden–Julian Oscillation (MJO), El Niño–Southern Oscillation (ENSO) teleconnections, and the austral-summer monsoon during the anomalously wet spring and summer of 2010 – 11.



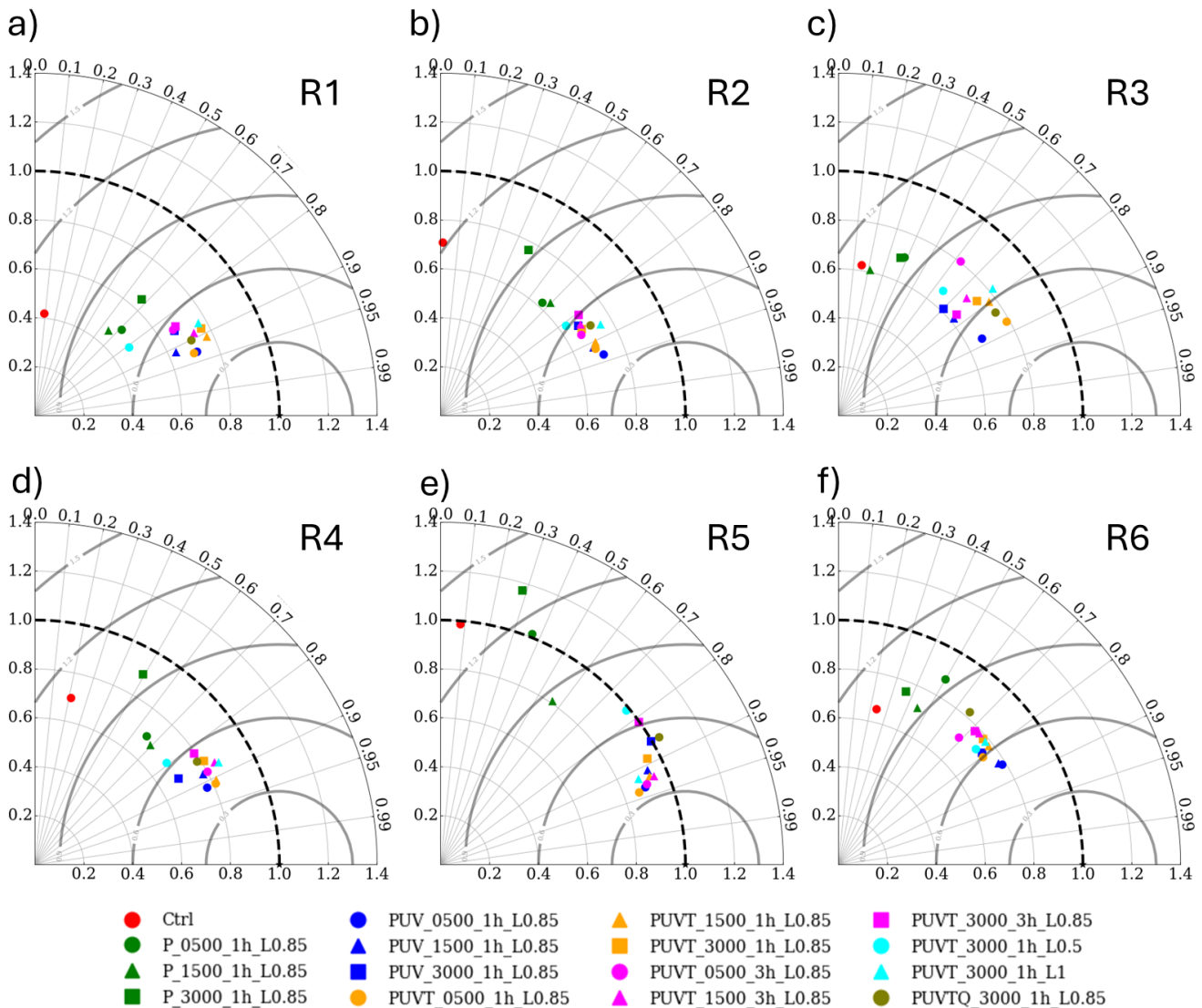


165 **Figure 2 (a) The averaged precipitation from December 2010 to March 2011 over the study domain (mm day<sup>-1</sup>) for IMERG; and (b)–(q) the bias between 16 simulations described in Table 1.**

The averaged IMERG precipitation exceeded 25 mm day<sup>-1</sup> over the MC and the western Pacific, with enhanced across northern and northeastern Australia (Fig. 2a). In contrast, central and southern Australia received less than 5 mm day<sup>-1</sup>. In general, IMERG, GPCP, and CMORPH exhibit similar spatial distributions (Fig. S1) and timeseries (Fig. S2), capturing the broad rainfall patterns during the extreme 2010 – 11 La Niña. The only notable difference is that IMERG tends to have 170 slightly more intense precipitation, particularly in the tropical region (R1) and over the Gulf of Carpentaria (R4) compared to GPCP and CMORPH.

In the CCAM simulations, the *Ctrl* displays substantial regional biases relative to IMERG (Fig. 2b). A wet bias (green shading) dominates the equatorial western Pacific, suggesting an excessive convective activity north of Papua New Guinea, while a dry bias (red shading) prevails across northern and eastern Australia, the MC, indicating a systematic 175 underestimation of tropical convection activities. Over Australia, the *Ctrl* shows strong dry biases (>5 mm day<sup>-1</sup>) in the north and similar, though less pronounced, bias in the southeast, underscoring the challenges in reproducing observed precipitation (Fig. 2b). The time series of spatially averaged daily rainfall for IMERG and AGCD over Australia shows strong agreement ( $r = 0.94$ ), with similar timing and intensity of rainfall events throughout the study period (Fig. S3), although IMERG is almost always wetter than AGCD, which may slightly reduce the dry bias.

180 Most nudged simulations reduce these continental biases, with biases over Australia generally constrained within  $\pm 2$  mm day<sup>-1</sup> (Fig. 2c-q). Improvements are most pronounced in the eastern and southern subregions, where large dry biases in the *Ctrl* are substantially diminished. However, model performance remains limited in specific regions, such as the wet bias observed in the high-elevation areas of Papua New Guinea and the dry bias over the Gulf of Carpentaria. These biases coincide with significant observational uncertainties (Alexander et al., 2020), as the three precipitation products differ 185 markedly in their representation of precipitation in region R3 and R4 (Fig. S1). These results suggest that while spectral nudging substantially improves rainfall representation over continental Australia, it is less effective in correcting tropical precipitation biases, which may be linked to convective parameterization and/or the impacts of horizontal resolution.



190 **Figure 3** Taylor diagrams of daily precipitation averaged from December 2010 to March 2011 for six subregions (R1–R6), comparing 16 CCAM simulations with IMERG. Radial axis (distance from origin) represents standard deviation of the simulated precipitation (normalized by the observed standard deviation, IMERG). Angular axis (angle from x-axis) represents correlation coefficient between models and IMERG. Solid gray concentric arcs represent the centered root-mean-square error (RMSE) between model and IMERG [a distance from the reference point on x-axis at (1,0)]. Coloured markers denote simulation groups (legend).

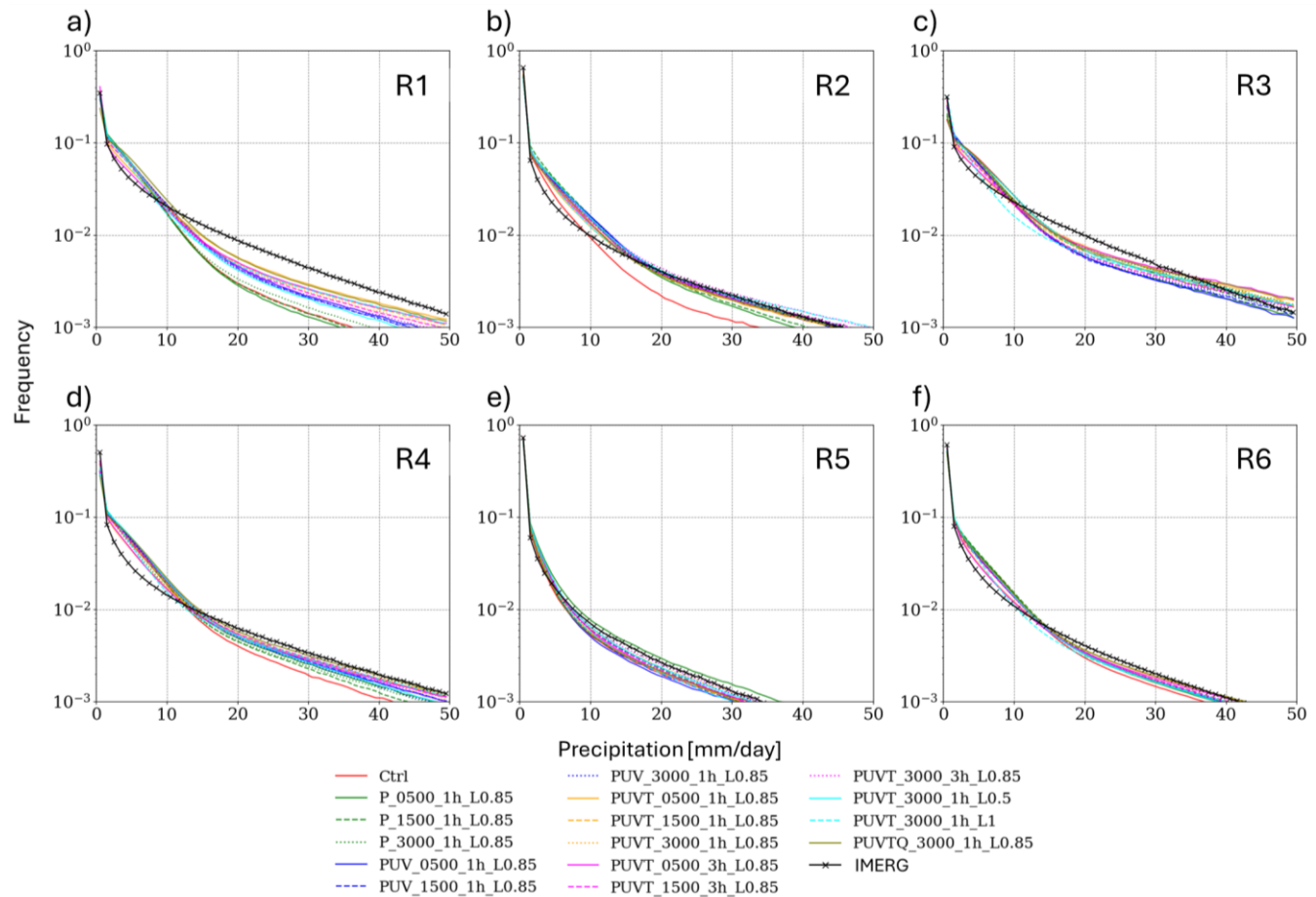
195

We used a Taylor diagram of mean precipitation distribution across six subregions (Fig. 3) to quantify spatial skill in terms of correlation (R), normalized standard deviation (nSD), and root-mean-square error (RMSE). The *Ctrl* shows very low correlations ( $R = 0.05 - 0.25$ ), strongly underestimated variance across all domains ( $nSD \sim 0.2 - 0.4$ ), and RMSE



consistently largest across all regions, underscoring its inability to reproduce the spatial-organized precipitation. In contrast,  
200 most nudged simulations achieved substantially higher skill, with  $R$  values of 0.80 – 0.95, nSD between 0.5 and 0.9, and markedly reduced RMSE. Improvements were most pronounced over Australian continent (R2, R4, and R5), where several configurations reached  $R \geq 0.9$  and nSD close to 1, while performance was weaker in convective (R1) and orographic (R3) regions, where  $R$  remained somewhat lower ( $\sim 0.75$  – 0.85) and RMSE larger. It is also worth mentioning that observational uncertainties are significant in estimating both mean precipitation and extremes in R1 and R3 (Nguyen et al., 2020;  
205 Alexander et al., 2020), which could explain the “weaker performance” observed in simulations over these regions.

Examining further into each nudged simulations indicate that  $P_{var}$  groups yields modest improvements over Australia. Furthermore, correlations remain weak in convective and orographic regions (e.g., R1, R3), rarely exceeding  $R = 0.6$  and with relatively large RMSE.  $PUV$  groups performs better, especially in R4 and R5 where correlations approach 0.9 and RMSE is reduced, though tropical biases persist. The  $PUVT\_1h$  and  $PUVT\_3h$  groups produce the most balanced results,  
210 with  $R$  consistently  $\geq 0.8$  – 0.9, nSD less than 1, and lowest RMSE across regions, particularly for shorter wavelength, 1-h updates (500 – 1500 km, L0.85). By contrast, simulations with adding moisture ( $PUVTQ$ ) or vertical levels ( $PUVT\_L$ ) exhibit inconsistent performance across regions, sometimes improving correlation but often at the cost of reduced variance. Collectively, these results align with previous discussion that shorter wavelength, frequent, multi-variable nudging ( $PUVT$ ) offers better spatial representation of precipitation, whereas vertical nudging of either from surface or mid- to the top of the  
215 atmosphere lead to regionally biased outcomes. Our analysis of the Taylor diagram comparing CCAM simulations to GPCP produced results similar to those obtained with IMERG, reinforcing our previous conclusion without altering the overall findings (Fig. S4).

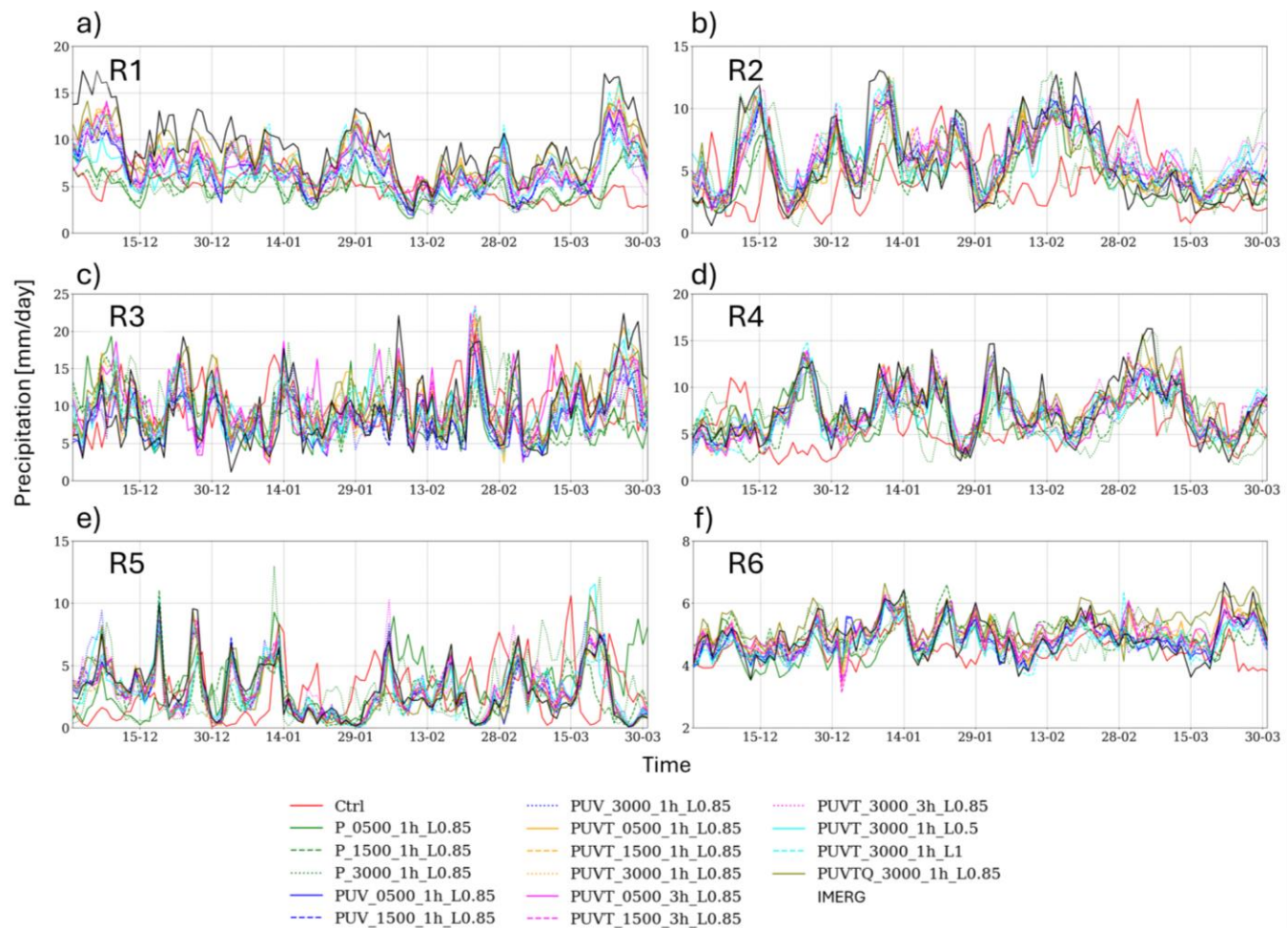


220 **Figure 4 Frequency of daily precipitation intensity for IMERG observation and 16 CCAM simulations averaged over each region from December 2010 to March 2011.**

We examined the frequency distributions of daily precipitation across six subregions (Fig. 4) to evaluate model fidelity relative to IMERG. All simulations overestimate light precipitation ( $5 - 15 \text{ mm day}^{-1}$ ) and underestimate moderate events ( $15 - 30 \text{ mm day}^{-1}$ ), with the largest discrepancies in R1 and R3 (Figs. 4a and c). R5 is the only region where light-rainfall biases are minimal. The frequency of extremes ( $>40 \text{ mm day}^{-1}$ ) is reasonably reproduced across all simulations. Improvements from nudging are most evident in R2 and R4 in all nudged simulations. In contrast, light rain excess remains persistent in R1 and R3, underscoring the difficulty of correcting convective and orographic rainfall biases even under optimized nudging configurations.



### 3.1.2 Temporal variance of precipitation



230

**Figure 5** Time series of spatially averaged daily rainfall (mm day<sup>-1</sup>) for IMERG and 16 CCAM simulations over six from December 2010 to March 2011.

Across all regions, the *Ctrl* simulation persistently underestimates rainfall (e.g., ~10 mm day<sup>-1</sup> deficit in R4 on 25 December 2010) while occasionally exaggerating daily peaks (e.g., >12 mm in R2 on 1 March 2011) (Fig. 5). It often fails to reproduce the timing of major events such as severe tropical cyclone Carlos over Darwin (15 February 2011, in Fig. 5b) and Yasi over Queensland (02 February 2011, in Fig. 5d). Nudged simulations substantially improve both timing and magnitude, reducing errors to ~1 – 5 mm day<sup>-1</sup>. Depending on nudging configurations, some runs (e.g., *P\_1500\_1h\_L0.85*) slightly underestimate peak intensities by 1 – 2 mm day<sup>-1</sup>. The largest improvements occur in R1 and R4, where *Ctrl* underestimates of ~10 mm day<sup>-1</sup> are reduced to <1.5 mm day<sup>-1</sup> in the best-performing *PUVT* runs, consistent with Taylor diagrams (Fig. 3) showing



240 correlations rising from ~0.5 in the *Ctrl* to >0.9 with nudging. The persistent underestimation in R1 through the entire timeseries may partly reflect its lower horizontal resolution (e.g., > 20 km, Fig. 1) relative to IMERG.  
The best overall performance is delivered by the *PUVT\_1h* group at 500 – 1500 km with short update intervals (1h, L0.85),  
which closely track the IMERG time series in R1 – R4, correcting peak errors of 10 mm day<sup>-1</sup> to <1.5 mm day<sup>-1</sup> while  
245 maintaining realistic phase alignment of major synoptic events. Moderate skill is achieved by the *PUVT\_3h* group and *PUV*  
runs, which improve timing and magnitude in some regions but degrade performance in others. In contrast, adding moisture  
or applying mid- or full-column nudging does not provide clear benefits, and in some cases degrades performance. The  
poorest outcomes are seen in the *Ctrl* and *P\_var* groups, which either sustain exaggerated peaks (>15 mm day<sup>-1</sup>) or distort  
the temporal structure.

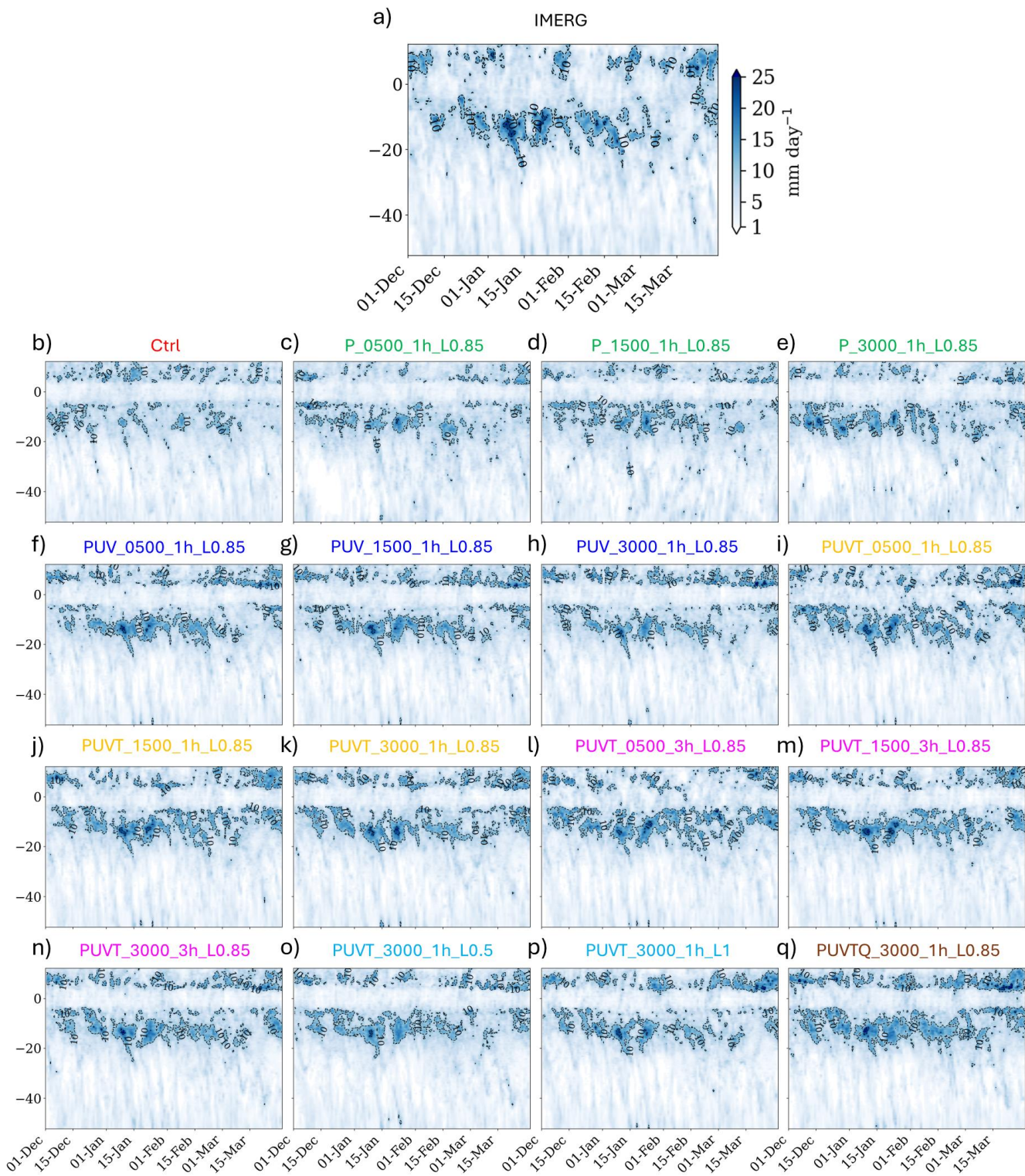




**Figure 6 Hovmöller diagram of zonally averaged daily precipitation (mm day<sup>-1</sup>) from the IMERG dataset for the period 1 December 2010 to 31 March 2011, averaged over 90°E to 170°E.**

The Hovmöller diagram of zonally averaged daily precipitation (Fig. 6) highlights the dominant influence of the MJO on rainfall variability during December 2010 – March 2011. IMERG indicates persistent convective maxima within  $\sim 15^{\circ}\text{S} - 15^{\circ}\text{N}$ , punctuated by two strong episodes in mid-January and early February 2011 with daily zonal means exceeding 25 mm day<sup>-1</sup> (Fig. 6a). These surges coincide with active MJO phases over the MC and western Pacific (RMM phases 4 – 7) (Fig. S5), consistent with the enhanced precipitation in the regional time series (Fig. 5) for R1–R4. However, the *Ctrl* fails to reproduce the intensity and spatial coherence of these convective maxima (Fig. 6b). Precipitation within  $15^{\circ}\text{S}-15^{\circ}\text{N}$  is markedly weaker, with zonal means rarely exceeding 10 mm day<sup>-1</sup>, and both major MJO surges are substantially underestimated. Convective regions appear fragmented and displaced, indicating the model's inability to capture the organized eastward propagation of MJO. South of  $20^{\circ}\text{S}$ , rainfall is sporadic and lacks the intensity and persistence evident in IMERG, consistent with the dry biases in the regional time series (Fig. 5). Collectively, these deficiencies demonstrate the *Ctrl*'s limited skill in representing tropical intraseasonal variability and its teleconnections across the MC and Australasian domain.

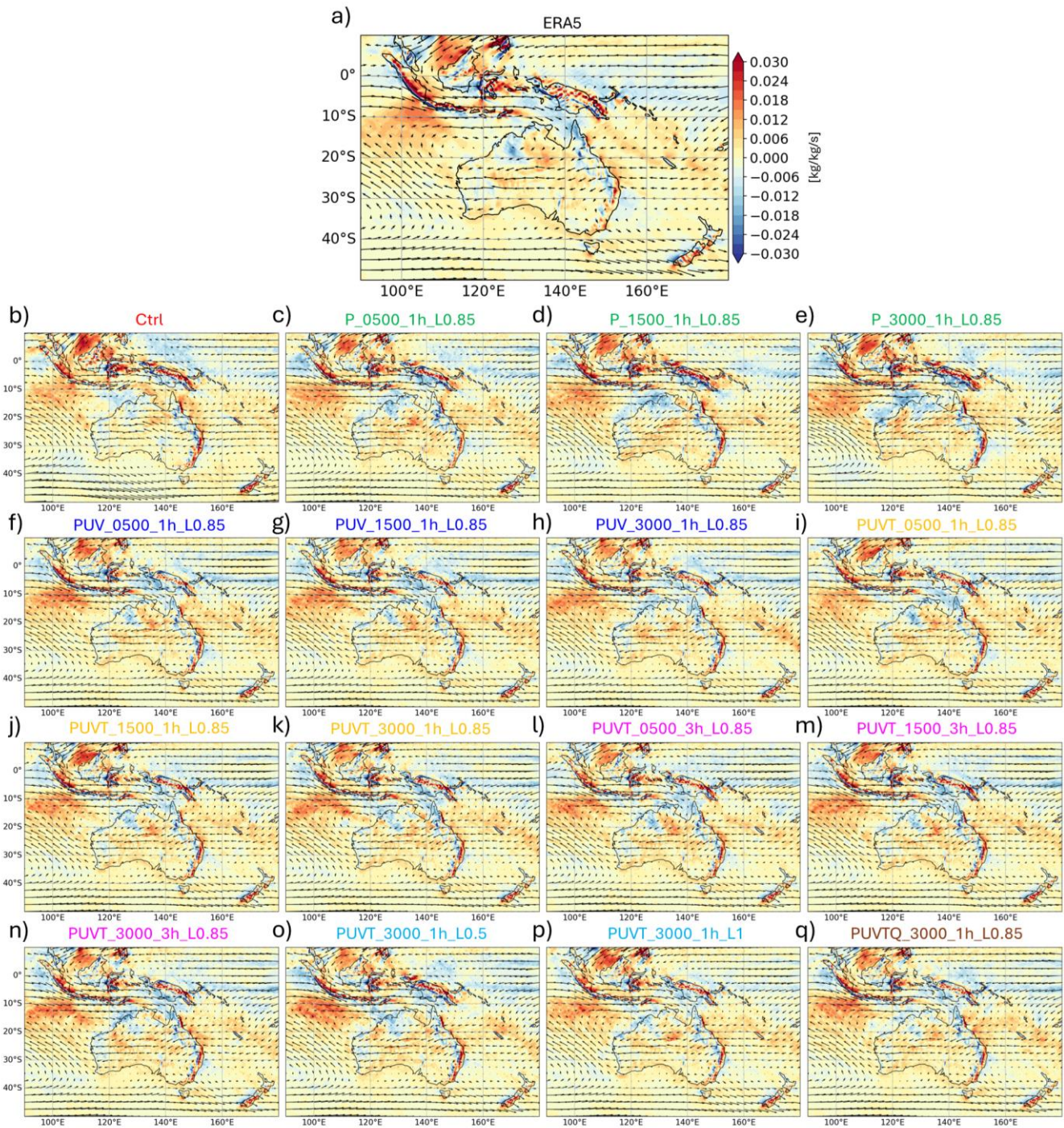
Nudged simulations markedly improve the zonal-mean representation of tropical precipitation compared to the *Ctrl* (Fig. 6c–q). Across most configurations, convective maxima within  $15^{\circ}\text{S} - 15^{\circ}\text{N}$  are intensified and better aligned with the MJO-related surges in mid-January and early February 2011, reducing the dry bias evident in the *Ctrl*. The *PUVT\_1h* group at short wavelengths (e.g., 500 – 1500 km, Fig. 6) perform best, capturing both the magnitude and spatial coherence of the convective regions and closely tracking the eastward propagation of MJO. *PUV* and *PUVT\_3h* runs also provide noticeable improvements in timing and magnitude, though their maxima are somewhat weaker than observed. Furthermore, configurations with mid-column nudging degrades model performance to represent MJO (Fig. 6o) whereas nudging from the surface to the top of the atmosphere does not add further benefit compared to other *PUVT* nudged simulations (Fig. 6p). The inclusion of specific humidity exaggerates light rainfall while failing to represent the organized MJO surges (Fig. 6q).

### 3.1.3 Low-level circulation and vertical correlation

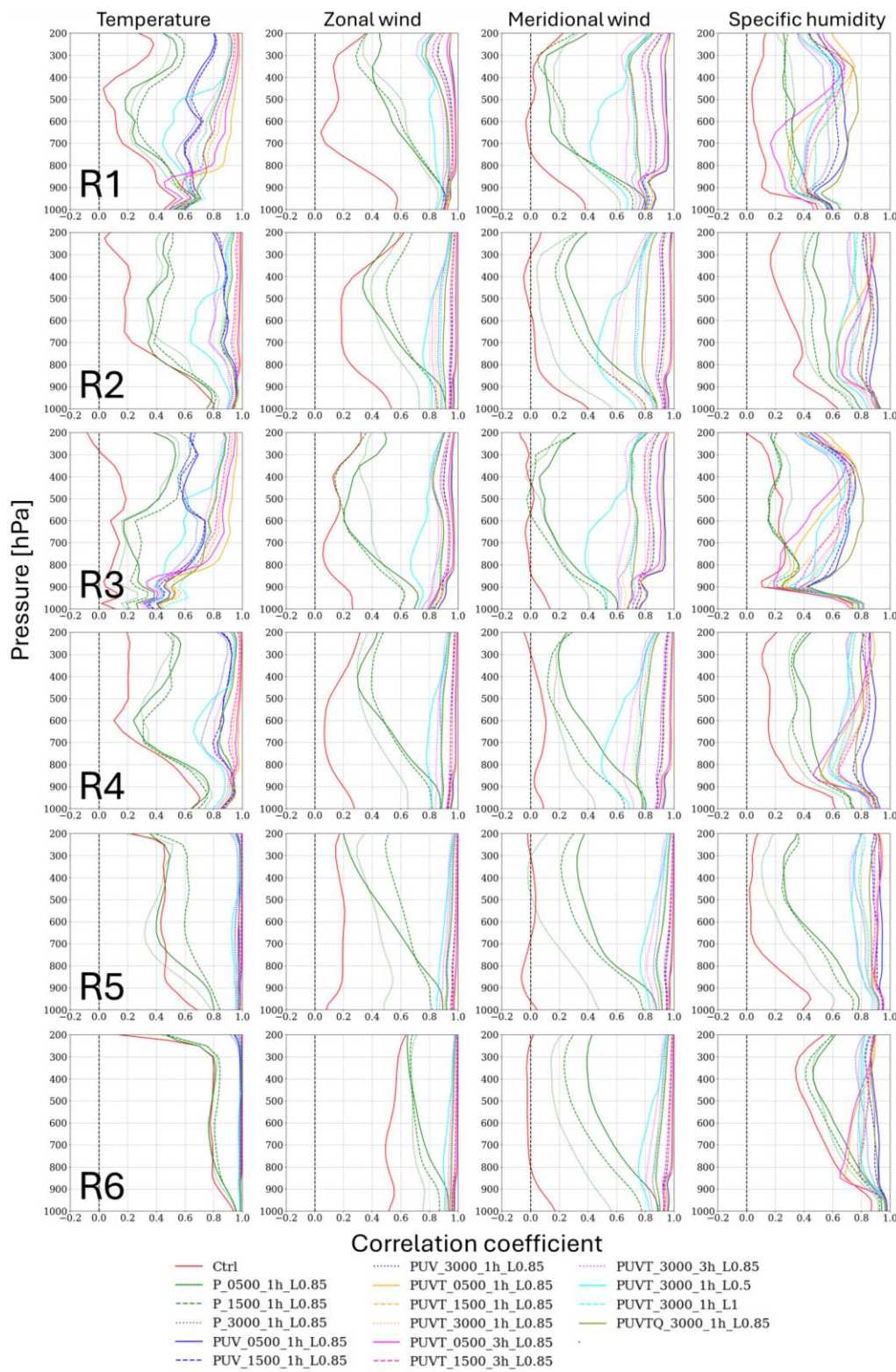
The analysis of moisture flux divergence from ERA5 data (Fig. 7) reveals distinct spatial patterns during the 2010 – 2011 La Niña event. A prominent convergence zone (blue shading) is observed over northern and northwest Australia (Fig. 7a), closely aligned with the low-pressure system in this region (Fig. S6). Subtropical divergence (red shading) south of approximately  $30^{\circ}\text{S}$  reflects subsidence, associated with a high-pressure system to the south (Fig. S6), which likely contributes to suppressed rainfall over southern Australia, consistent with the observed decrease in precipitation shown in Fig. 1a. Low-level wind patterns indicate monsoonal winds from the tropics, driving moisture towards the Australian continent, a feature consistent with the active Australian monsoon during this period (e.g., BoM, 2012; Giles, 2012; Lisonbee and Ribbe 2021). The convergence regions identified in Fig. 7a qualitatively correspond to high-precipitation areas, particularly over the Gulf of Carpentaria, west of Sumatra, New Guinea, the MC, and New Zealand (Fig. 1a). In



contrast, the *Ctrl* exhibits a weaker and displaced low-pressure system over northwest Australia, resulting in diminished  
285 moisture convergence and an underestimation of precipitation in those regions such as the Gulf of Carpentaria, as seen in  
Fig. 1a. These discrepancies highlight the limitations of the *Ctrl* in accurately capturing monsoonal dynamics. In contrast,  
the nudged simulations significantly improve both the spatial structure and magnitude of moisture convergence, as well as  
290 the low-level circulation. The inclusion of pressure nudging (Fig. 7c-e) enhances the representation of low- and high-  
pressure systems over Australia, with the low-pressure system over northwest Australia becoming more defined and  
accurately positioned relative to the *Ctrl*. The inclusion of  $u$  and  $v$  wind nudging in *PUV* (Fig. 7f-h) and *PUVT* (Fig. 7i-n)  
simulations greatly enhance monsoonal wind flow towards Australia, improving moisture convergence in regions such as the  
Gulf of Carpentaria and New Guinea, and aligning moisture flux divergence more closely with observed precipitation  
patterns, especially at shorter wavelengths (e.g., *PUVT\_0500\_1h\_L0.85* and *PUVT\_1500\_1h\_L0.85*). Quantitatively, the  
location and magnitude of convergence regions over northern Australia improve by ~30 – 40% compared to the *Ctrl*. It is  
295 important to note that nudging is not applied below 850 hPa, except for in the *PUVT\_3000\_1h\_L1* case; however, similar  
improvements in moisture transport and convergence are observed at 875 hPa. There is minimal difference in moisture  
transport and convergence between cases where nudging is applied from 500 hPa (mid-troposphere to top of the atmosphere)  
and from the surface to the top of the atmosphere. However, when moisture nudging is included, additional convergence  
regions emerge, particularly over northern and western Australia, which corresponds to the overestimated rainfall observed  
300 in Fig. 5f and 6q.



**Figure 7** The averaged wind fields (vectors) and water vapor flux divergence (color shades; unit) from ERA5 at 875 hPa from December 2010 to March 2011 over study domain; (a) ERA5 and (b)–(q) the corresponding plot for the 16 CCAM simulations.





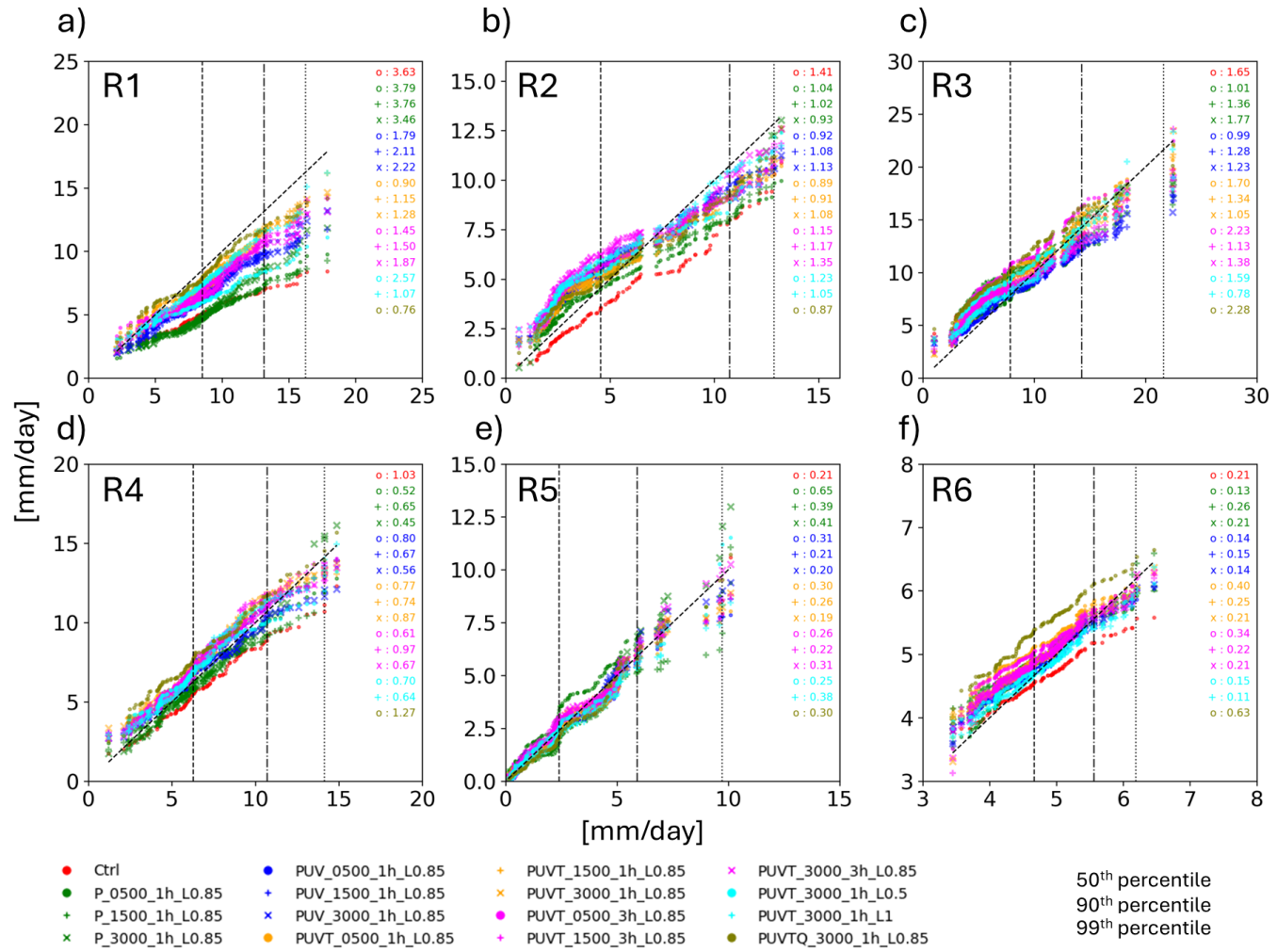
**Figure 8** Vertical profiles of the correlation coefficient for the spatial pattern of Temperature,  $U$  wind component,  $V$  wind component, specific humidity from top to bottom 16 CCAM simulations against ERA from December 2010 to March 2011 over 6 regions R1 to R6 from left to right.

Figure 8 presents vertical correlations of temperature ( $t$ ), zonal wind ( $u$ ), meridional wind ( $v$ ), and specific humidity ( $q$ ) 310 between 16 CCAM simulations and ERA5 across the six subregions (R1 – R6). The *Ctrl* run exhibits the weakest skill, with correlations frequently below 0.4 in the mid- to upper troposphere (400–200 hPa). Nudged simulations markedly improve vertical coherence, although the magnitude of improvement varies by configurations. For temperature, the *PUVT\_1h* group, particularly, *PUVT\_0500\_1h\_L0.85* and *PUVT\_1500\_1h\_L0.85* simulations achieve correlations exceeding 0.8, whereas mid-column nudging (*PUVT\_3000\_1h\_L0.5*) degrades the simulated temperature skill and full-column nudging 315 (*PUVT\_3000\_1h\_L1*) offers no additional benefit, reinforcing the concept of constraining above the boundary layer while allowing near-surface fields to evolve freely. For winds, correlations in the *Ctrl* remain weak (<0.5) throughout much of the troposphere, consistent with its poor representation of monsoon inflow and subtropical divergence (Fig. 7b). Nudged simulations, particularly *PUV* and *PUVT* at 500 – 1500 km, raise correlations to 0.7 – 0.9 across most levels, although values 320 remain lower in the upper troposphere over R1 and R3. Specific humidity shows the greatest variability. In the *Ctrl*, correlations drop largely above 700 hPa (<0.2 in R1–R3), while *PUVT\_0500\_1h\_L0.85* and *PUVT\_1500\_1h\_L0.85* improve to 0.6 – 0.8 in the mid-troposphere. Although nudging moisture (*PUVTQ\_3000\_1h\_L0.85*) enhances the simulated specific humidity, the correlation does not differ significantly from other nudged simulations that do not include moisture nudging (Fig. 8).

Regionally, R1 and R3 remain problematic even with nudging, as the vertical correlations for temperature and specific 325 humidity in near the surface and aloft remain weaker, consistent with persistent rainfall biases (Fig. 2, 4). By contrast, R4 and R5 show the largest improvement across all four variables (Fig. 8), aligning with improved magnitude and event timing of precipitation in Figs. 5–6. Domain-wide vertical correlation (R6, rightmost in Fig. 8) further suggests that nudged runs consistently outperforming the *Ctrl* across all variables.



330 3.2 Extreme precipitation



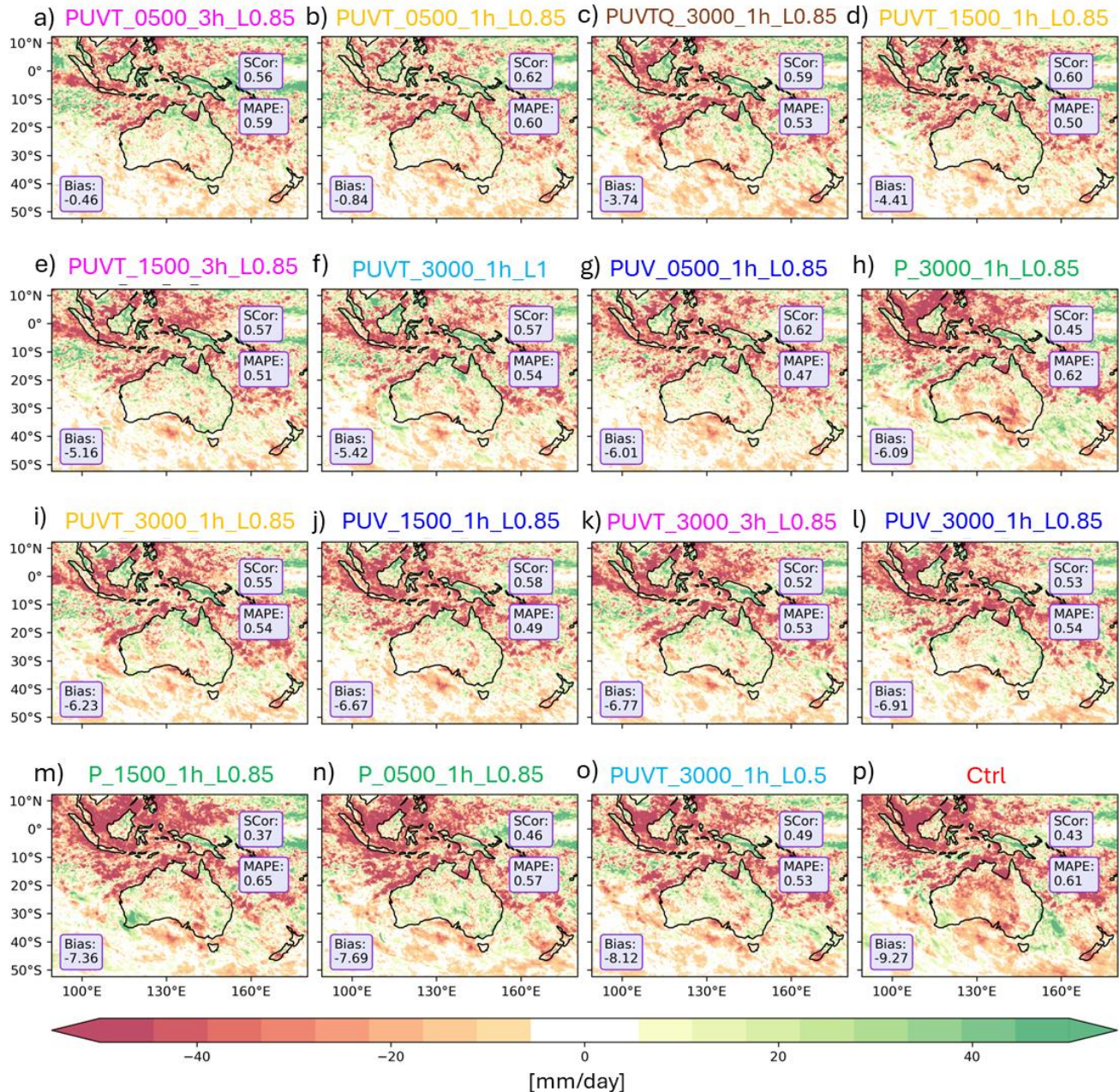
335 **Figure 9** Quantile-quantile plots of regionally averaged daily precipitation (mm day<sup>-1</sup>) against IMERG for six subregions. Coloured symbols denote different CCAM simulations (see legend). The dashed 1:1 line represents perfect agreement with observations. The numbers indicate the area formed by the 1:1 and model line. Numbers on the top right of each panel indicate the area between IMERG and CCAM in which the larger the number the larger difference between the two.

Figure 8 shows quantile – quantile (QQ) plots of daily regionally averaged precipitation against IMERG for the six subregions. The *Ctrl* shows the largest departures from the 1:1 line, systematically underestimating rainfall beyond the median (50<sup>th</sup> percentile) and failing to capture heavy rainfall above the 99<sup>th</sup> percentile in most regions, particularly R1, R2, R4, and whole domain, R6, consistent with its dry biases observed in Figs. 2 and 6. Nudged simulations substantially improves the precipitation distribution, with the best agreement achieved by *PUVT\_1h* group (orange marker in Fig. 9).



These configurations reduce mean biases to < 1 mm/day across all regions and closely follows IMERG up to the 90<sup>th</sup> percentile, while also reproducing the upper tail of the distribution (99<sup>th</sup>) more realistically, including the balance of extremes in R2-R5. It also stands out to be the best configuration for R1 region despite the coarse horizontal resolution.

345 *PUVT\_3h* group performs nearly as well, though with slightly scatter beyond the 90<sup>th</sup> percentile. It is interesting to note that the shorter wavelength (e.g., 500 and 1500 km) runs reduce biases substantially and follow IMERG closely through the 90<sup>th</sup> percentile, remaining stable without under- or overshooting. In contrast, longer-wavelength configurations (e.g., 3000 km) remain acceptable up to the 90<sup>th</sup> percentile but tend to under- or overshoot high-quantile rainfall thereafter, particularly in R3, R4, and R5, with normalized biases of ~3 – 5 mm/day. In contrast, moisture nudging (*PUVTQ\_3000\_1h\_L0.85*) shows 350 the largest biases, significantly increases rainfall above all percentiles (Fig. 9f). This is consistent with its degraded frequency distributions (Fig. 4f) and overestimation of zonally averaged daily precipitation (Fig. 6q). A persistent limitation across all simulations is the underestimation of the very highest extremes (above the 99.9<sup>th</sup> percentile) in R1 and R3, even in the best *PUVT* runs, reflecting unresolved convective and orographic processes. Overall, these diagnostics confirm that low-level, high-frequency *PUVT* nudging at intermediate wavelengths (500 – 1500 km, L0.85) provides the most balanced 355 performance, reducing systematic biases across the distribution, from the median through the 90<sup>th</sup> percentile, while preserving realistic variability at higher quantiles whereas weaker (e.g., only pressure nudging) or over-constrained configurations (e.g., adding moisture) either fail to correct or exacerbate extremes.



360 **Figure 10. Bias of monthly maximum 1-day precipitation ( $Rx1day$ ;  $mm day^{-1}$ ) from December 2010 to March 2011 relative to IMERG. Each panel shows one CCAM spectral nudging simulation (see labels), with shading indicating spatial bias across the CORDEX-Australasia domain. Statistics included in each panel are the spatial correlation (SCor), mean absolute percentage error (MAPE), and domain-averaged bias.**

Figure 10 illustrates the bias of monthly maximum 1-day precipitation ( $Rx1day$ ) from December 2010 to March 2011, comparing 16 CCAM simulations to IMERG. Although the study period is relatively short, it is considered representative



365 due to the extreme wet conditions associated with the 2010–2011 La Niña event. It is noteworthy that Alexander et al.,  
(2025) used a combination of in situ, satellite, and reanalysis data to evaluate precipitation extremes (Rx1day) over land  
from 2001 to 2015 and found significant variability among the products in estimating regional annual wettest days. For  
instance, IMERG over land tends to be wetter than the Asian Precipitation -Highly Resolved Observational Data Integration  
Towards Evaluation of Water Resources (APHRODITE; Yatagai et al., 2012) over Monsoon Asia. Nevertheless, IMERG is  
370 used as the "reference" to evaluate the Rx1day from CCAM simulations in our analysis.

Figure 10 presents panels (a) to (p) arranged from the wettest to the driest simulations, where negative values (red) indicate  
dry biases (underestimation), and positive values (green) denote wet biases (overestimation) of extreme rainfall. The results  
reveal substantial variations in simulation performance. The *Ctrl* and *P\_var* consistently fail to capture extreme rainfall, with  
Scor values  $\leq 0.46$ , MAPEs  $\geq 0.57$ , and significant underestimations (-7 to -9 mm day $^{-1}$ ). *PUV* and *PUVT* group at longer  
375 wavelength (e.g., 3000 km), demonstrate reasonable skill but still suffer from large dry biases ( $>-6$  mm day $^{-1}$ ). In contrast,  
configurations at shorter wavelengths (e.g., *PUVT\_0500\_1h\_L0.85* with Scor = 0.62, MAPE = 0.60, Bias = -0.84) perform  
better, minimizing the dry bias over the sea of MC. However, they overestimate precipitation over land regions such as  
Borneo, Papua New Guinea, and northern Australia.

The overestimation over northern Australia is plausible, as IMERG tends to be drier than AGCD over the Australian  
380 continent (Alexander et al., 2025, Figs. 6 and S25). In contrast, the land regions of the MC require further validation against  
reliable in situ observations. Overall, these rankings reinforce that short-wavelength (500 – 1500 km), low-level nudging of  
pressure, winds and temperature provides the most reliable representation of extremes.

#### 4 Discussion and Conclusion

This study evaluated the sensitivity of Conformal Cubic Atmospheric Model (CCAM) regional climate simulations to  
385 different spectral nudging (SN) configurations during the extreme 2010 – 11 La Niña event. The assessment aimed to  
examine the model's ability to reproduce large-scale circulation and regional precipitation patterns, quantify the impact of  
nudging settings on mean and extreme rainfall, and identify optimal configurations to enhance simulation fidelity.

Our evaluation demonstrates that spectral nudging has a decisive influence on the model's ability to reproduce both mean  
and extreme precipitation across Australasia. However, the effectiveness of nudging varies depending on the set of variables  
390 used, the selected wavelength, and the nudging update frequency. We found that shorter wavelength, high-frequency  
nudging of pressure, winds, and temperature, provides the best balance between maintaining large-scale fidelity and allowing  
for regional variability. This configuration consistently minimized rainfall biases (Figs. 2–4) and best captured the timing  
and intensity of major extreme precipitation events, such as severe tropical cyclone Cat 5 – Carlos over Darwin and Yasi  
over Queensland, while also reproducing the MJO phase (Fig. 5). It further reproduced realistic moisture convergence into  
395 northern Australia and wind flow consistent with the monsoon (Fig. 6). Additionally, it aligned well with ERA5 vertical  
structures (Fig. 7) and produced accurate quantile distributions of extreme rainfall (Figs. 8–9). This result is consistent with



previous studies (e.g., Thatcher and McGregor, 2008; Tang et al., 2017; Spero et al., 2018), which have highlighted the effectiveness of scale-selective nudging in constraining large-scale circulation while preserving mesoscale variability and extreme events.

400 The wavelength of the nudging plays a crucial role in determining model performance. By selecting a cut-off wavelength around 500 – 1500 km, we effectively nudged the synoptic scale of the model solution while still allowing for the development of finer-scale features. This range aligns with the findings of Gómez and Miguez-Macho (2017), who identified 405 1000 km as an optimal wavelength for nudging in their study. Additionally, the update frequency of 1 hour for nudging aligns with previous studies (Liu et al., 2012; Otte et al., 2012), ensuring a high degree of consistency between the nudged model and the large-scale atmospheric fields. The vertical level at which nudging is applied also influences model skill. In this study, the best performance was achieved with nudging applied above 850 hPa, consistent with findings by Wang and Kotamarthi (2013) and von Storch et al. (2000). We found that adding moisture nudging degrades the model's representation 410 of mean and extreme precipitation, consistent with previous studies that caution against its use due to potential thermodynamic inconsistencies (Heikkila et al., 2010; Liu et al., 2012), although some studies have reported improvements in rainfall statistics (Omrani et al., 2015). Configurations with longer wavelengths (e.g., 3000 km) or infrequent nudging 415 updates (e.g., 3h) led to smoother rainfall fields, weaker extremes, and misaligned convergence zones (Fig. 3–6). This sensitivity mirrors previous studies that show overly strong or infrequent nudging degrades model performance by weakening large-scale forcing and impacting regional variability (Alexandru et al., 2009; Omrani et al., 2015). In summary, our study demonstrates that applying spectral nudging on large-scale fields above the planetary boundary layer can 420 significantly improve the simulation of mean and extremes in CCAM over Australasia. We recommend using configurations with moderate nudging wavelengths (~500 – 1500 km), short relaxation times (~1h), and including pressure, wind, and temperature nudging for the most accurate simulations of mean and extreme rainfall. In our study, the “PUVT\_0500\_1h\_L0.85” configuration achieved the highest skill across multiple diagnostics, successfully preserving large-scale circulation fidelity while allowing mesoscale processes to evolve.

425 While the application of spectral nudging in this study has significantly improved the simulation of large-scale circulation and extreme precipitation events, several limitations remain. Firstly, despite the improved performance of the nudged model, biases persist, particularly over tropical convective and mountainous regions, where the model underestimates extreme precipitation at the 99<sup>th</sup> percentile. These persistent biases indicate that, although spectral nudging improves model accuracy, missing or inadequately represented regional physical processes limit the simulation of extreme precipitation, especially in 430 complex orographically influenced regions. It is important to note, however, that observational products also exhibit deficiencies in these areas, which adds uncertainty to our model performance assessment. The study's 12 km horizontal resolution, while suitable for capturing mesoscale processes, may still miss finer-scale features like localized convection that influence extreme rainfall, and higher resolutions could provide a more accurate representation of these processes. Additionally, the 4-month simulation period during the extreme wet summer of 2010 – 11 offers valuable insights, but the results are limited to this event. The model's performance over different climate periods, particularly drier or less extreme



seasons, may differ, suggesting that future research could expand the time frame of simulations to assess variability and robustness across various climate conditions. The impact of GCM biases, which can propagate into the RCM simulation (Liu et al., 2024; Liang et al., 2008), remains another area for future research, particularly in integrating bias correction techniques or multi-model ensembles to enhance the fidelity of RCM projections. Our study contributes to the growing body 435 of work on spectral nudging and its potential for enhancing regional climate simulations, particularly for applications in climate risk assessment and adaptation planning.

### Author contribution

ST designed the study, carried out the analysis, and wrote the initial manuscript draft. MJT, PLN, LVA, and JLM provided supervision and contributed to manuscript review and revisions.

### 440 Competing interest

The contact author has declared that none of the authors has any competing interests.

### Acknowledgement

We would also like to thank the CSIRO HPC (Petrichor) for the computational resources.

### Financial support

445 This work is supported by the Australian Climate Service. PLN and LVA are supported by Australian Research Council (ARC) grant FT210100459. LVA is also supported by ARC grant CE230100012.

### Code and data availability

The CCAM model code, version CCAM-2504, is fully open source and made available by CSIRO at (<https://github.com/csiro/ccam-ccam/>). The model post-processing code is available at (<https://github.com/csiro/ccam-pcc2hist>). The ERA5 hourly data on single levels from 1940 to present can be downloaded from <https://doi.org/10.24381/cds.bd0915c6> (Hersbach et al., 2023). The Global Precipitation Climatology Project (GPCP) daily CDR v3.2 (Huffman et al., 2023) can be downloaded at <https://doi.org/10.1175/JCLI-D-23-0123.1> and <https://www.ncei.noaa.gov/data/global-precipitation-climatology-project-gpcp-daily/access/>. The Climate Prediction Center morphing method (CMORPH) v1.0 CRT (Joyce et al., 2004; Xie et al., 2017) can be downloaded at 455 [https://doi.org/10.1175/1525-7541\(2004\)005<0487:CAMTPG>2.0.CO;2](https://doi.org/10.1175/1525-7541(2004)005<0487:CAMTPG>2.0.CO;2) and <https://www.ncei.noaa.gov/data/cmorph-high-res-global-precipitation-access/>



resolution-global-precipitation-estimates/. The Integrated Multi-Satellite Retrievals for the Global Precipitation Measurement IMERG Final Run product (Version 07; Huffman et al., 2019), distributed by NASA GES DISC can be downloaded at <https://doi.org/10.5067/GPM/IMERGDF/DAY/06> and [https://disc.gsfc.nasa.gov/datasets/GPM\\_3IMERGDF\\_07/summary](https://disc.gsfc.nasa.gov/datasets/GPM_3IMERGDF_07/summary). All figures presented in this manuscript were generated 460 using Python scripts, which are publicly available at (<https://doi.org/10.5281/zenodo.18423588>). All references of the datasets are listed in the in-text data citation references.

## Reference

Alexandru, A., de Elía, R., Laprise, R., Separovic, L., & Biner, S. (2009). Sensitivity study of regional climate model simulations to large-scale nudging parameters. *Monthly Weather Review*, 137(5), 1666–1686.  
465 <https://doi.org/10.1175/2008MWR2620.1>

Alexander, L. V., and Coauthors, 2025: Less intense daily precipitation maxima in regional compared to global gridded products. *J. Climate*, <https://doi.org/10.1175/JCLI-D-25-0222.1>, in press.

Alexander, L. V., Bador, M., Roca, R., Contractor, S., Donat, M. G., and Nguyen, P. L.: Intercomparison of annual precipitation indices and extremes over global land areas from in situ, space-based and reanalysis products, *Environ. Res. Lett.*, 15, 055002, <https://doi.org/10.1088/1748-9326/ab79e2>, 2020.  
470

BoM (2012). Record-breaking La Niña events: An analysis of the La Niña life cycle and the impacts and significance of the 2010–11 and 2011–12 La Niña events in Australia. Bureau of Meteorology, Commonwealth of Australia.

Cai, W., & van Rensch, P. (2012). The 2011 southeast Queensland extreme summer rainfall: A confirmation of a shift in the interdecadal Pacific oscillation? *Geophysical Research Letters*, 39(8), L08702. <https://doi.org/10.1029/2011GL050820>

475 Castro, C. L., Pielke Sr, R. A., & Leoncini, G. (2005). Dynamical downscaling: Assessment of value retained and added using the Regional Atmospheric Modeling System (RAMS). *Journal of Geophysical Research*, 110(D5), D05108. <https://doi.org/10.1029/2004JD004721>

Cha, D. H., Jin, C. S., Lee, D. K., & Kuo, Y. H. (2011). Impact of intermittent spectral nudging on regional climate simulation using WRF. *Journal of Geophysical Research: Atmospheres*, 116(D10), D10103.  
480 <https://doi.org/10.1029/2010JD015069>

Chapman, S., Syktus, J., Trancoso, R., Toombs, N. & Eccles, R. Projected changes in mean climate and extremes from downscaled high-resolution CMIP6 simulations in Australia. *Weather and Climate Extremes* 46, 100733, <https://doi.org/10.1016/j.wace.2024.100733> (2024).

Choi SJ, Lee DK. 2015. Impact of spectral nudging on the downscaling of tropical cyclones in regional climate simulations.  
485 *Adv. Atmos. Sci.* 33: 730–742.

Evans, J. P., Boyer-Souchet, I., & Olson, R. (2012). Local sea surface temperatures add to extreme precipitation in northeast Australia during La Niña. *Geophysical Research Letters*, 39(10), L10803. <https://doi.org/10.1029/2012GL052014>



Evans, J. P., Marchand, R., & Ackerman, T. (2014). Variability of Australian monsoon precipitation in the last 60 years. *Journal of Climate*, 27(15), 5859–5870. <https://doi.org/10.1175/JCLI-D-13-00422.1>

490 Feser, F. (2012). Regional climate models add value to global model data: A review and selected examples. *Environmental Research Letters*, 7(1), 014024. <https://doi.org/10.1088/1748-9326/7/1/014024>

Feser, F., and M. Barcikowska (2012), The influence of spectral nudging on typhoon formation in regional climate models, *Environ. Res. Lett.*, 7(1), 14,024.

495 Freidenreich, S. M., and V. Ramaswamy. 1999. “A New Multiple-Band Solar Radiative Parameterization for General Circulation Models.” *Journal of Geophysical Research: Atmospheres* 104: 31389–31409.

Giorgi, F. (2019). Thirty years of regional climate modeling: Where are we and where are we going next? *Journal of Geophysical Research: Atmospheres*, 124(11), 5696–5723. <https://doi.org/10.1029/2018JD030094>

Giorgi, F., & Mearns, L. O. (1999). Introduction to special section: Regional climate modeling revisited. *Journal of Geophysical Research: Atmospheres*, 104(D6), 6335–6352. <https://doi.org/10.1029/98JD02072>

500 Gibson, P. B., Lewis, H., Campbell, I., Rampal, N., Fauchereau, N., & Harrington, L. J. (2025). Downscaled climate projections of tropical and ex-tropical cyclones over the southwest Pacific. *Journal of Geophysical Research: Atmospheres*, 130, e2025JD043833. <https://doi.org/10.1029/2025JD043833>

Gibson, P.B., Stuart, S., Sood, A. et al. Dynamical downscaling CMIP6 models over New Zealand: added value of climatology and extremes. *Clim Dyn* 62, 8255–8281 (2024). <https://doi.org/10.1007/s00382-024-07337-5>

505 Giles, B.D. (2012), The Australian Summer 2010/2011. *Weather*, 67: 9–12. <https://doi.org/10.1002/wea.860>

Gómez, B. and Miguez-Macho, G. (2017), The impact of wave number selection and spin-up time in spectral nudging. *Q.J.R. Meteorol. Soc.*, 143: 1772–1786. <https://doi.org/10.1002/qj.3032>

Grose, M. R., Narsey, S., Delage, F., Dowdy, A. J., Bador, M., Boschat, G., et al. (2020). Insights from CMIP6 for Australia’s future climate. *Earth’s Future*, 8(5), e2019EF001469. <https://doi.org/10.1029/2019EF001469>

510 Heikkila, U., Sandvik, A., and Sorteberg, A.: Dynamical downscaling of ERA-40 in complex terrain using the WRF regional climate model, *Clim. Dynam.*, 37, 1551–1564, <https://doi.org/10.1007/s00382-010-0928-6>, 2010.

Hersbach, H., Bell, B., Berrisford, P., Hirahara, S., Horányi, A., Muñoz-Sabater, J., Nicolas, J., Peubey, C., Radu, R., Schepers, D., Simmons, A., Soci, C., Abdalla, S., Abellán, X., Balsamo, G., Bechtold, P., Biavati, G., Bidlot, J., Bonavita, M., De Chiara, G., Dahlgren, P., Dee, D., Diamantakis, M., Dragani, R., Flemming, J., Forbes, R., Fuentes, M., Geer, A., 515 Haimberger, L., Healy, S., Hogan, R. J., Hólm, E., Janisková, M., Keeley, S., Laloyaux, P., Lopez, P., Lupu, C., Radnoti, G., de Rosnay, P., Rozum, I., Vamborg, F., Villaume, S., and Thépaut, J.-N.: The ERA5 global reanalysis, *Q. J.R. Roy. Meteor. Soc.*, 146, 1999–2049, <https://doi.org/10.1002/qj.3803>, 2020.

Hersbach, H., Bell, B., Berrisford, P., Biavati, G., Horányi, A., Muñoz Sabater, J., Nicolas, J., Peubey, C., Radu, R., Rozum, I., Schepers, D., Simmons, A., Soci, C., Dee, D., and Thépaut, J.-N.: ERA5 hourly data on pressure levels from 1940 to 520 present, Copernicus Climate Change Service (C3S) Climate Data Store (CDS) [data set], <https://doi.org/10.24381/cds.bd0915c6>, 2023.



Hoffmann, P., Katzfey, J.J., McGregor, J.L., Thatcher, M., 2016. Bias and variance correction of sea surface temperatures used for dynamical downscaling. *J. Geophys. Res. Atmos.* 121 (21), 12877–812890. <https://doi.org/10.1002/2016JD025383>.

Huffman, G. J., Stocker, E. F., Bolvin, D. T., Nelkin, E. J., & Tan, J. (2019). GPM IMERG final precipitation L3 1 day 0.1 degree x 0.1 degree V06. In A. Savtchenko & M. D. Greenbelt (Eds.), Goddard earth sciences data and information services center (GES DISC). <https://doi.org/10.5067/GPM/IMERGDF/DAY/06>

Huffman, G. J., R. F. Adler, A. Behrangi, D. T. Bolvin, E. J. Nelkin, G. Gu, and M. R. Ehsani, 2023: The New Version 3.2 Global Precipitation Climatology Project (GPCP) Monthly and Daily Precipitation Products. *J. Climate*, 36, 7635–7655, <https://doi.org/10.1175/JCLI-D-23-0123.1>.

525 Hurley, P. 2007. “Modelling Mean and Turbulence Fields in the Dry Convective Boundary Layer With the Eddy-Diffusivity/Mass-Flux Approach.” *Boundary-Layer Meteorology* 125: 525–536. <https://doi.org/10.1007/s10546-007-9203-8>.

Hong, S. Y., & Chang, E. C. (2012). Spectral nudging sensitivity simulations in a regional climate model. *Asia-Pacific Journal of Atmospheric Sciences*, 48(4), 345–355. <https://doi.org/10.1007/s13143-012-0033-3>

535 Imran, H.M., Evans, J.P. Observational uncertainty in the added value of regional climate modelling over Australia. *Clim Dyn* 63, 73 (2025). <https://doi.org/10.1007/s00382-024-07562-y>

Isphording, R. N., Alexander, L. V., Bador, M., Green, D., Evans, J. P., and Wales, S.: A Standardized Benchmarking Framework to Assess Downscaled Precipitation Simulations, *J. Climate*, 37, 1089–1110, <https://doi.org/10.1175/JCLI-D-23-0317.1>, 2024.

540 IPCC, 2021: Climate Change 2021: The Physical Science Basis. Contribution of Working Group I to the Sixth Assessment Report of the Intergovernmental Panel on Climate Change. Cambridge University Press, Cambridge, United Kingdom and New York, NY, USA, In press, doi:10.1017/9781009157896.

Jin, C. S., Cha, D. H., Lee, D. K., Suh, M. S., Hong, S. Y., Kang, H. S., & Ho, C. H. (2016). Evaluation of climatological tropical cyclone activity over the western North Pacific in the CORDEX-East Asia multi-RCM simulations. *Climate Dynamics*, 47(3), 765–778. <https://doi.org/10.1007/s00382-015-2869-6>

545 Joyce, R. J., J. E. Janowiak, P. A. Arkin, and P. Xie, 2004: CMORPH: A Method that Produces Global Precipitation Estimates from Passive Microwave and Infrared Data at High Spatial and Temporal Resolution. *Journal of Hydrometeorology*, 5, 487-503 (DOI: 10.1175/1525-7541(2004)005<0487:CAMTPG>2.0.CO;2).

Jones, D. A., W. Wang, and R. Fawcett, 2009: High-quality spatial climate data-sets for Australia. *Aust. Meteor. Oceanogr. J.*, 58, 233–248, <https://doi.org/10.22499/2.5804.003>.

550 Kanamitsu, M., & Kanamaru, H. (2007). Fifty-seven-Year California reanalysis downscaling at 10 km (CaRD10). Part I: System detail and validation with observations. *Journal of Climate*, 20(22), 5553–5571. <https://doi.org/10.1175/2007JCLI1482.1>



555 Liang, X.-Z., K. E. Kunkel, G. A. Meehl, R. G. Jones, and J. X. L. Wang (2008), Regional climate models downscaling analysis of general circulation models present climate biases propagation into future change projections, *Geophys. Res. Lett.*, 35, L08709, doi:10.1029/2007GL032849.

Liu, S., Zeman, C., & Schär, C. (2024). Dynamical downscaling of climate simulations in the tropics. *Geophysical Research Letters*, 51, e2023GL105733. <https://doi.org/10.1029/2023GL105733>

560 Liu, Y. L., Alexander, L. V., Evans, J. P., & Thatcher, M. (2024). Sensitivity of Australian rainfall to driving SST datasets in a variable-resolution global atmospheric model. *Journal of Geophysical Research: Atmospheres*, 129, e2024JD040954 <https://doi.org/10.1029/2024JD040954>

Liu P, Tsimpidi AP, Hu Y, Stone B, Russell AG, Nenes A. 2012. Differences between downscaling with spectral and grid nudging using WRF. *Atmos. Chem. Phys.* 12: 3601–3610. <https://doi.org/10.5194/acp-12-3601-2012>.

565 Lisonbee, J. and Ribbe, J.: Seasonal climate influences on the timing of the Australian monsoon onset, *Weather Clim. Dynam.*, 2, 489–506, <https://doi.org/10.5194/wcd-2-489-2021>, 2021.

Ma, S., Trancoso, R., Syktus, J., Chapman, S., & Eccles, R. (2025). Evaluating ERA5 downscaled simulations using CCAM: Large-scale circulation processes and teleconnections. *Journal of Geophysical Research: Atmospheres*, 130, e2025JD043566. <https://doi.org/10.1029/2025JD043566>

570 McGregor, J. L. 2003. “A New Convection Scheme Using a Simple Closure.” *BMRC Research Report* 93: 33–36.

McGregor, J. L., and M. R. Dix. 2008. “An Updated Description of the Conformal-Cubic Atmospheric Model.” In *High Resolution Numerical Modelling of the Atmosphere and Ocean*, edited by K. Hamilton and W. Ohfuchi. Springer. [https://doi.org/10.1007/978-0-387-49791-4\\_4](https://doi.org/10.1007/978-0-387-49791-4_4).

Miguez-Macho, G., G. L. Stenchikov, and A. Robock, 2004: Spectral nudging to eliminate the effects of domain position and geometry in regional climate model simulations. *J. Geophys. Res.*, 109, D13104, <https://doi.org/10.1029/2003JD004495>.

575 Menut, L., Bessagnet, B., Cholakian, A., Siour, G., Mailler, S., and Pennel, R.: What is the relative impact of nudging and online coupling on meteorological variables, pollutant concentrations and aerosol optical properties?, *Geosci. Model Dev.*, 17, 3645–3665, <https://doi.org/10.5194/gmd-17-3645-2024>, 2024.

Narsey S et al. (2025) Disentangling the uncertainties in regional projections for Australia. *Journal of Southern Hemisphere Earth Systems Science* 75, ES25015. doi:10.1071/ES25015

580 Nguyen, P. L., Alexander, L. V., Thatcher, M. J., Truong, S. C. H., Ispahonding, R. N., and McGregor, J. L.: Selecting CMIP6 global climate models (GCMs) for Coordinated Regional Climate Downscaling Experiment (CORDEX) dynamical downscaling over Southeast Asia using a standardised benchmarking framework, *Geosci. Model Dev.*, 17, 7285–7315, <https://doi.org/10.5194/gmd-17-7285-2024>, 2024.

Nguyen, P.-L., Bador, M., Alexander, L. V., Lane, T. P., and Ngo-Duc, T.: More intense daily precipitation in CORDEX-SEA regional climate models than their forcing global climate models over Southeast Asia, *Int. J. Climatol.*, 42, 6537–6561, <https://doi.org/10.1002/joc.7619>, 2022



Nguyen, P.-L., Bador, M., Alexander, L. V., Lane, T. P., and Funk, C. C.: On the Robustness of Annual Daily Precipitation Maxima Estimates Over Monsoon Asia, *Frontiers in Climate*, 2, 578785, <https://doi.org/10.3389/fclim.2020.578785>, 2020

Otte, T. L., Nolte, C. G., Otte, M. J., and Bowden, J. H.: Does Nudging Squelch the Extremes in Regional Climate  
590 Modeling?, *J. Climate*, 25, 7046–7066, <https://doi.org/10.1175/JCLI-D-12-00048.1>, 2012.

Omrani, H., Drobinski, P., Dubos, T., & Turuncoglu, U. U. (2015). Optimal nudging strategies in regional climate modeling: Investigation in a Big-Brother simulation over the Euro-Mediterranean region. *Climate Dynamics*, 44(5–6), 1559–1577. <https://doi.org/10.1007/s00382-014-2453-5>

Rotstayn, L. D., and U. Lohmann. 2002. “Simulation of the Tropospheric Sulfur Cycle in a Global Model With a Physically  
595 Based Cloud Scheme.” *Journal of Geophysical Research: Atmospheres* 107, no. D21: AAC 20-1–AAC 20-21. <https://doi.org/10.1029/2002JD002128>.

Schroeter, B. J. E., B. Ng, A. Takbash, T. Rafter, and M. Thatcher, 2024: A Comprehensive Evaluation of Mean and Extreme Climate for the Conformal Cubic Atmospheric Model (CCAM). *J. Appl. Meteor. Climatol.*, 63, 997–1018, <https://doi.org/10.1175/JAMC-D-24-0004.1>.

600 Schwarzkopf, M. D., and V. Ramaswamy. 1999. “Radiative Effects of CH<sub>4</sub>, N<sub>2</sub>O, Halocarbons and the Foreign-Broadened H<sub>2</sub>Ocon-Tinuum: A GCM Experiment.” *Journal of Geophysical Research: Atmospheres* 104: 9467–9488.

Spero, T. L., Nolte, C. G., Bowden, J. H., & Mallard, M. S. (2018). Sensitivity of WRF simulations to different spectral nudging techniques. *Journal of Applied Meteorology and Climatology*, 57(6), 1303–1320. <https://doi.org/10.1175/JAMC-D-17-0098.1>

605 Spero, T. L., Otte, M. J., Bowden, J. H., and Nolte, C. G.: Improving the representation of clouds, radiation, and precipitation using spectral nudging in the Weather Research and Forecasting model, *J. Geophys. Res.-Atmos.*, 119, 11682–11694, <https://doi.org/10.1002/2014JD022173>, 2014.

Tang, J., Song, S., & Wu, J. (2009). Impacts of the spectral nudging technique on simulation of the East Asian summer monsoon. *Theoretical and Applied Climatology*, 101(1–2), 41–51. <https://doi.org/10.1007/s00704-009-0202-1>

610 Tang, J., Wang, S., Niu, X., Hui, P., Zong, P., & Wang, X. (2017). Impact of spectral nudging on regional climate simulation over CORDEX East Asia using WRF. *Climate Dynamics*, 48(7–8), 2339–2357. <https://doi.org/10.1007/s00382-016-3208-2>

Thatcher, M., & McGregor, J. L. (2008). Using a scale-selective filter for dynamical downscaling with the conformal cubic atmospheric model. *Monthly Weather Review*, 136(2), 4578–4596. <https://doi.org/10.1175/2008MWR2599.1>

Thatcher, M., and P. Hurley. 2012. “Simulating Australian Urban Climate in a Mesoscale Atmospheric Numerical Model.”  
615 *Boundary Layer Meteorology* 142: 149–175.

Truong, S. C. H., Ramsay, H. A., Rafter, T., & Thatcher, M. J. (2025). Simulation of an intense tropical cyclone in the conformal cubic atmo-spheric model and its sensitivity to horizontal resolution. *Weather and Climate Extremes*, 47, 100744. <https://doi.org/10.1016/j.wace.2025.100744>

Truong, S. C. H., & Thatcher, M. (2025). Evaluation of clouds in the conformal cubic atmospheric model using the CFMIP  
620 observation simulator package. *International Journal of Climatology*, 45(8), e8846. <https://doi.org/10.1002/joc.8846>



Ummenhofer, C. C., Sen Gupta, A., Briggs, P. R., England, M. H., McIntosh, P. C., Meyers, G. A., et al. (2015). How did ocean warming affect Australian rainfall extremes during the 2010–2011 La Niña event? *Geophysical Research Letters*, 42(3), 9942–9951. <https://doi.org/10.1002/2015GL065947>

von Storch, H., Langenberg, H., & Feser, F. (2000). A spectral nudging technique for dynamical downscaling purposes.

625 Monthly Weather Review, 128(10), 3664–3673. [https://doi.org/10.1175/1520-0493\(2000\)128<3664:ASNTFD>2.0.CO;2](https://doi.org/10.1175/1520-0493(2000)128<3664:ASNTFD>2.0.CO;2)

Wang J, Kotamarthi VR. 2013. Assessment of dynamical downscaling in near-surface fields with different spectral nudging approaches using the nested regional climate model (NRCM). *J. Appl. Meteorol. Climatol.* 52: 1576–1591. <https://doi.org/10.1175/JAMC-D-12-0302.1>.

Xie, P., R. Joyce, S. Wu, S. Yoo, Y. Yarosh, F. Sun, and R. Lin, 2017: Reprocessed, Bias-Corrected CMORPH Global High-630 Resolution Precipitation Estimates from 1998. *J. Hydrometeor.*, 18, 1617–1641 (DOI: 10.1175/JHM-D-16-0168.1).

Yatagai, A., K. Kamiguchi, O. Arakawa, A. Hamada, N. Yasutomi, and A. Kitoh, 2012: APHRODITE: Constructing a Long-Term Daily Gridded Precipitation Dataset for Asia Based on a Dense Network of Rain Gauges. *Bull. Amer. Meteor. Soc.*, 93, 1401–1415, <https://doi.org/10.1175/BAMS-D-11-00122.1>.

Yhang, Y. B., & Hong, S. Y. (2011). A study on large-scale nudging effects in regional climate model simulation. *Asia-635 Pacific Journal of Atmospheric Sciences*, 47(3), 235–243. <https://doi.org/10.1007/s13143-011-0012-0>